nanomaterials

MDPI

Article

On the Mechanism of the Oxygen Reduction Reaction on Nitrogen-Doped Graphenes in Alkaline Media

Vitaliy Kislenko *, Sergey Pavlov, Petr Chekushkin and Sergey Kislenko *

Joint Institute for High Temperatures of the Russian Academy of Sciences, Izhorskaya St. 13 Bd.2, 125412 Moscow, Russia

* Correspondence: vitaly.kislenko@gmail.com (V.K.); kislenko@ihed.ras.ru (S.K.)

Abstract

Nitrogen-doped graphene-like materials exhibit high catalytic activity and stability in the oxygen reduction reaction. DFT-based theoretical studies of catalytic activity typically assume that the reaction proceeds via an inner-sphere mechanism involving chemisorption of an oxygen molecule. In this work, using grand-canonical DFT calculations, we demonstrate that, in an alkaline medium, an outer-sphere mechanism, initiated by an electron transfer to a solvated O_2 molecule near the surface, is energetically more favorable. On N-doped graphene containing graphitic nitrogen atoms, the reaction proceeds via a 4e mechanism due to a significant reduction in the chemisorption energy of the *OH intermediate, whereas on pristine graphene the reaction terminates after two electron transfers.

Keywords: graphene; oxygen reduction reaction; mechanism; DFT; MD

1. Introduction

The landmark article by Gong et al. [1], which first demonstrated the catalytic activity of N-doped nanotubes in the oxygen reduction reaction (ORR), launched a new line of research—metal-free carbon-based electrocatalysts (CMFECs)—that continues to attract interest to this day [2,3]. Among the wide variety of CMFECs, N-doped carbon materials are the most extensively studied to date. They are less effective in acidic media due to a relatively high overpotential and insufficient stability for the ORR, specifically as a result of the protonation of nitrogen atoms [4–6]. In alkaline media, N-doped carbon exhibits an onset potential comparable to that of Pt catalyst, while surpassing it in stability [1,7,8], which is a subject of significant interest.

Despite extensive research, data on the catalytic mechanism of nitrogen impurities and the rate-determining step of the ORR remain contradictory. DFT calculations serve as the primary theoretical tool for investigating these issues. In most cases, regardless of the medium pH, a so-called associative inner-sphere mechanism is assumed. It begins with the adsorption/chemisorption of an O_2 molecule at the catalytic site, followed by its reduction via a series of concerted electron–proton transfers involving the sequential formation of the chemisorbed intermediates *OOH, *O, and *OH [8–14]. In an alkaline medium, this mechanism is typically represented as follows:

Academic Editor: Gregory M. Odegard

Received: 26 October 2026
Revised: 17 November 2026
Accepted: 20 November 2026
Published: 23 November 2026

Copyright: © 2026 by the authors. Licensee MDPI, Basel, Switzerland. This article is an open access article distributed under the terms and conditions of the Creative Commons Attribution (CC BY) license.

$$O_2 + * \rightarrow *O_2 \quad (1)$$

$$*O_2 + H_2O + e \rightarrow *OOH + OH^- \quad (2)$$

$$*OOH + e \rightarrow *O + OH^- \quad (3)$$

$$*O + H_2O + e \rightarrow *OH + OH^- \quad (4)$$

$$*OH + e \rightarrow OH^- \quad (5)$$

Although nitrogen impurities significantly lower the dissociation barrier of the O_2 molecule [15,16], the dissociative mechanism of the ORR remains more energetically demanding [11] and is usually not considered.

The thermodynamics of the associative inner-sphere mechanism can be calculated using standard DFT with the computational hydrogen electrode model. By assuming concerted electron–proton transfer in each elementary step, one can avoid the explicit modeling of charged reactants/products and express the sum of free energies $G(H^+) + G(e)$ (or the sum $G(H_2O) - G(OH^-) + G(e)$ for alkaline conditions) in terms of $G(H_2)$ [11,17]. In our view, this technical feature explains the widespread prevalence of this mechanism in theoretical studies.

In the study by Liang et al., an analysis of the associative mechanism for N-doped graphenes in an alkaline medium demonstrated that, for graphitic N atoms, reaction 4 is the rate-determining step [11]. In later studies, DFT calculations performed without explicitly accounting for water led to the conclusion that the formation of *OOH is the rate-determining step for graphitic N, whereas the desorption of *OH is the rate-determining step for pyridinic N [8,9]; at the same time, the O_2 adsorption/chemisorption stage was not considered. Standard DFT calculations are typically performed at zero surface charge, which can lead to significant errors in calculating the thermodynamic profiles of electrocatalytic reactions for two-dimensional materials [18,19]. For this reason, we employed grand-canonical (constant-potential) DFT calculations in our previous work. It was demonstrated that the chemisorption of O_2 on pristine graphene is a highly endothermic reaction (chemisorbed O_2 is a metastable state [20,21]), making it the rate-determining step [22,23]. Nitrogen impurities reduce the O_2 chemisorption energy, which is consistent with previous studies [11,22]. More interestingly, as the surface potential decreases to ~0 V vs. SHE, the O_2 chemisorption energy drops abruptly and continues to decrease as the potential shifts into the negative region [22,23], which can explain the catalytic effect of nitrogen impurities. In this case, the generally accepted mechanism of the ORR is disrupted, and the initial concerted electron–proton transfer (reaction 2) is replaced by sequential electron and proton transfers.

Despite the general acceptance of the associative inner-sphere mechanism, its validity for CMFECs is not so obvious. This mechanism implies that the onset potential of the oxygen reduction reaction (ORR) depends linearly on pH (on the SHE scale). This indeed holds true for Pt [24], whereas for N-doped carbon, the onset potential is independent of pH [25], similarly to what is observed for Au [26]. As noted by Koper in his review, this effect can arise from the decoupling of proton and electron transfer [27]—a phenomenon we previously observed for the O_2 adsorption reaction—which may explain the pH independence of the onset potential [28]. However, this effect can be explained by a completely different reaction mechanism, in which the first and rate-determining step is an outer-sphere electron transfer to a solvated oxygen molecule [27,29,30]:

$$O_2 + e \rightarrow O_2^- \quad (6)$$

An ORR mechanism for Au in an alkaline medium was previously developed by Schmickler's group, in which the first reaction is an outer-sphere electron transfer (6), while the subsequent steps are as follows: [31–34]:

$$O_2^- + H_2O + e \rightarrow OOH^- + OH^- \quad (7)$$

$$OOH^- + H_2O + * \rightarrow 2*OH + OH^- \quad (8)$$

$$2*OH + e \rightarrow *OH + OH^- \quad (9)$$

$$*OH + e \rightarrow OH^- \quad (10)$$

It was also noted that this mechanism is likely applicable to other catalysts in an alkaline medium that interact weakly with oxygen, such as Ag, mercury, and graphite. In this regard, using grand-canonical DFT calculations, we investigated the thermodynamics of the outer-sphere mechanism (6–10) and demonstrated that, for N-doped graphenes with graphitic nitrogen atoms, it is energetically more favorable than the inner-sphere one (1–5). Due to a reduction in the chemisorption energy of *OH intermediates, nitrogen impurities promote the ORR via a 4e mechanism, whereas on pristine graphene, oxygen reduction terminates after reaction (7), with the number of transferred electrons being 2.

2. Methods

2.1. Details of DFT Calculations

The simulation cell was represented by rectangular single-layer graphene with in-plane dimensions of 12.8 Å × 12.3 Å and a vacuum spacing of 15 Å in the direction perpendicular to the graphene plane. This study examined two systems: pristine graphene and graphene containing a single substitutional nitrogen defect (so-called graphitic nitrogen) (Figure 1). The nitrogen atom accounts for approximately 2% of the carbon atoms in the cell.

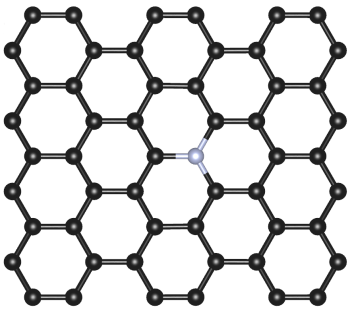

Figure 1. Snapshot of the simulation cell: graphene with a single substitutional nitrogen defect. C and N atoms are black and blue, respectively.

Spin-polarized DFT calculations were performed using the JDFTx software package (v1.7.0) [35]. The implicit aqueous electrolyte containing 1 M KCl was described by the CANDLE solvation model [36]. The GGA-PBE exchange–correlation functional [37], supplemented by the DFT-D3 van der Waals correction [38], was employed. The core electrons were described using GBRV ultrasoft pseudopotentials [39]. The kinetic energy cutoff for plane waves and charge density was 28 Ha and 140 Ha, respectively. A Gaussian-based (erfc) function with 0.001 Ha smearing width was used as a smearing function for the electronic fillings. The electronic energy convergence criterion was set to 10^{-8} Ha. During ionic optimization, the convergence thresholds for energy difference between successive iterations and for the root mean square of forces was 10^{-6} Ha and 10^{-6} Ha/Bohr, respectively. The Brillouin zone was sampled using a Gamma-centered 5 × 5 × 1 k-point

mesh. The convergence tests for the plane-wave cutoff and k-point sampling are shown in Figure S7 in the Supplementary Materials.

2.2. Active Sites

In our previous work, we investigated the most energetically favorable configurations of chemisorbed *O_2, *OOH, *O, and *OH intermediates corresponding to the inner-sphere mechanism of the ORR on N-doped graphene [22]. Briefly, for graphene containing graphitic N, the active binding sites for the intermediates are the carbon atoms adjacent to the nitrogen (Figure 2a–f). Nitrogen attracts electron density from its neighboring carbon atoms through the σ-bonding network. This makes the nearest-neighbor carbon positively charged (as illustrated in Figure S3 in the Supplementary Materials) and more reactive toward intermediates [40].

Two configurations are possible for the chemisorbed O_2 molecule, involving two bonds or one bond with the surface (Figures 2a and 2b, respectively). Which of these is stable and most energetically favorable depends on the graphene potential [22]. For the case of two chemisorbed OH* species (considered in the outer-sphere mechanism), the most energetically favorable configuration is shown in Figure 2f. Both hydroxyl groups are also bonded to carbon atoms adjacent to the nitrogen dopant. Only the configurations presented in Figure 2 were used to construct the free-energy profile for the oxygen reduction reaction. However, they were re-optimized for each potential value investigated in this study.

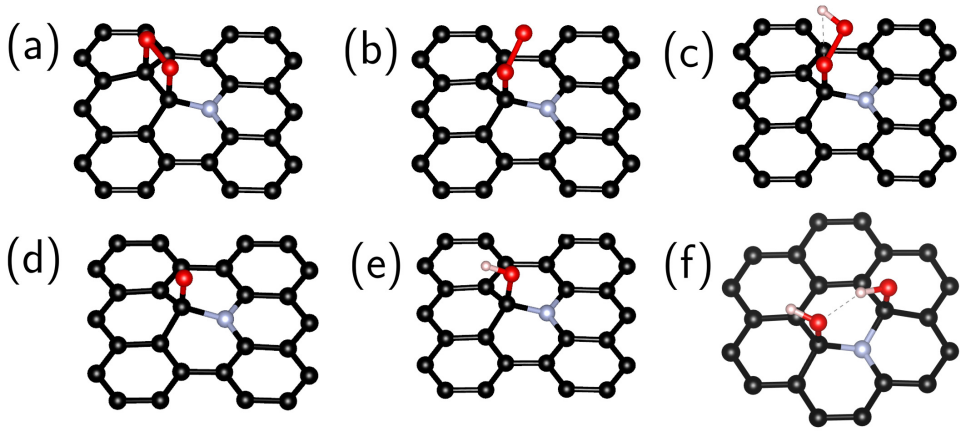

Figure 2. The lowest energy configurations of chemisorbed *O_2 (**a**,**b**), *OOH (**c**), *O (**d**), *OH (**e**), and 2*OH (**f**) for N-doped graphene. C, N, O, and H atoms are black, blue, red, and white, respectively.

2.3. Potential of Mean Force

To analyze the change in the free energy of an oxygen molecule as it moves from the bulk electrolyte to the surface, combined classical molecular dynamics (MD) simulations and DFT calculations were employed. Within the framework of MD simulations, an O_2 molecule in water near a graphene surface was considered, and the potential of mean force for the transfer of the molecule from the bulk water to the surface was calculated:

$$G_{MD}(x) = -\int_{bulk}^{x} \langle F(x) \rangle dx$$

where $\langle F(x) \rangle$ is the average force acting on a molecule at a distance x from the surface. In the MD simulations, O_2–H_2O, H_2O–H_2O, and H_2O–surface interactions were taken into account. The O_2–surface interaction was excluded because, at short distances, a chemical bond forms between the carbon atoms of the surface and the oxygen atoms of the O_2 molecule. The π-bond in the graphene is disrupted. The carbon atoms involved in the

chemical bond are displaced from the graphene plane, transitioning into a sp^3-hybridized state (Figure 2). It is impossible to describe both the energetic and configurational changes in such a system using simple pairwise interaction potentials. Therefore, the contribution from the O_2–surface interaction was accounted for through separate DFT calculations, in which the change in the system's energy $E_{DFT}(x)$ was determined as a function of the distance x between the surface and the O_2 molecule in a vacuum. The total energy profile was calculated as the sum of the contributions obtained from MD and DFT:

$$G(x) = E_{DFT}(x) + G_{MD}(x)$$

During the scan of the reaction coordinate x in both MD and DFT calculations, the orientation of the O_2 molecule was kept fixed. The O–O bond was parallel to the surface, directly above the surface binding sites, as shown in Figure 2a. In the DFT calculations, all surface atoms—except for those involved in bond formation—were held fixed; the O–O bond length and the spin state of the system were optimized at each value of x.

For the MD simulations, a force field developed in this work was used. In the case of N-doped graphene, the non-uniform charge distribution within the graphene sheet was taken into account. Details are provided in the Supplementary Materials.

2.4. Free Energy Profile Calculation for the ORR from GC-DFT

Let us consider reaction (2) as an example. Within the GC framework, the reaction free energy can be expressed as follows:

$$\Delta G_\mu = G_\mu(^*\mathrm{OOH}) + G(OH^-) - \left(G_\mu(^*\mathrm{O_2}) + G(\mathrm{H_2O}) + \Delta N \mu_e\right)$$

where ΔN is the difference between the number of electrons in the products and the reactants. The subscript μ indicates that the free energy is evaluated at a fixed electrochemical potential. The free energy of the OH^- ion was calculated using the following equation [41]:

$$G(H^+) + G(OH^-) = G(H_2O)$$

where $G(H^+)$ is given by:

$$G(H^+) = G(H^+; pH = 0) - 0.059 \cdot pH = G\left(H_{2(g)}\right) / 2 - \mu_e^{SHE} - 0.059 \cdot pH.$$

For the electrolyte model that we applied, $\mu_e^{SHE} = -4.66$ eV [41]. Throughout all calculations, the pH was set to 14.

The Gibbs free energy G includes vibrational, translational, and rotational energy in addition to the electronic energy obtained directly from DFT calculations. For graphene sheets with and without adsorbates, only the vibrational contribution was considered. For isolated molecules, translational and rotational contributions were also included, with the corresponding corrections evaluated for both the solvated and gas-phase molecules. The calculation procedure was the same as in our previous work (see Section S1 in the Supplementary Info. of Ref. [22] for a detailed description of vibrational/translational/rotational energy calculation).

3. Results and Discussion

3.1. Thermodynamics of Oxygen Transport from the Bulk of the Solution to the Graphene Surface

Figure 3 shows the potentials of mean force for an oxygen molecule as a function of the distance from pristine and N-doped graphene, obtained using combined MD and DFT calculations. Due to technical constraints, the calculation was performed only for the case of a zero net surface charge. As can be seen from the dependence of surface charge on potential (Figure 4), the potential of zero charge (PZC) for the systems under study is significantly more negative than the onset potential for the oxygen reduction reaction (ORR) on N-doped carbon catalysts, which is $E \sim 0$ V vs. SHE [7,25,42]. Therefore, the simulation

conditions correspond to a rapidly proceeding ORR. On an RDE polarization curve, this corresponds to the region where the current reaches its diffusion limit. Since the oxygen molecule is neutral, we assume that the PMF is not overly sensitive to the surface charge. To confirm this, we performed additional MD simulations for charged surfaces at a potential of $E = 0$. As shown in Figure S6 in Supplementary Materials, for pristine graphene the PMF is essentially the same at the PZC and $E = 0$. For N-doped graphene, there is some quantitative difference. However, the qualitative trend of increasing in the PMF as an oxygen molecule approaches the surface remains unchanged.

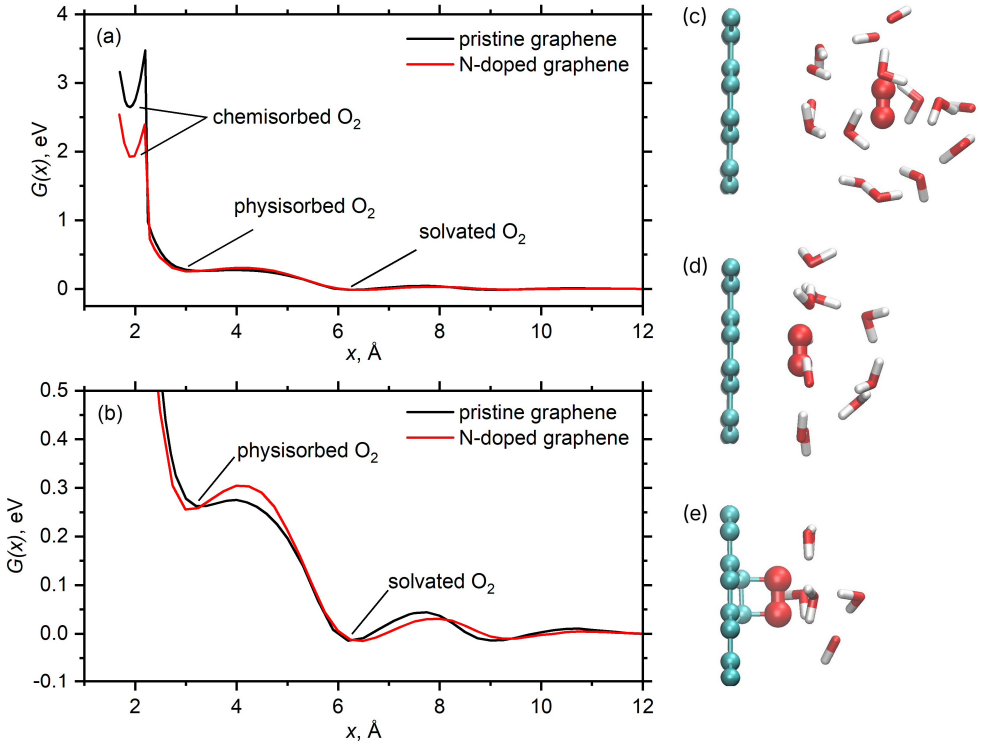

Figure 3. (**a**)—Potential of mean force for oxygen molecule as a function of the distance to the surface at the PZC; (**b**)—The same as in (**a**) but with a different scale on the energy axis (from −0.1 to 0.5 eV). Solvent-separated configuration and physisorbed and chemisorbed oxygen molecules are shown in (**c**), (**d**), and (**e**), respectively. Figures (**c**–**e**) show only those water molecules that are located at a distance of no more than 4 Å from the oxygen. C, O, and H atoms in (**c**), (**d**), (**e**) are cyan, red, and white, respectively.

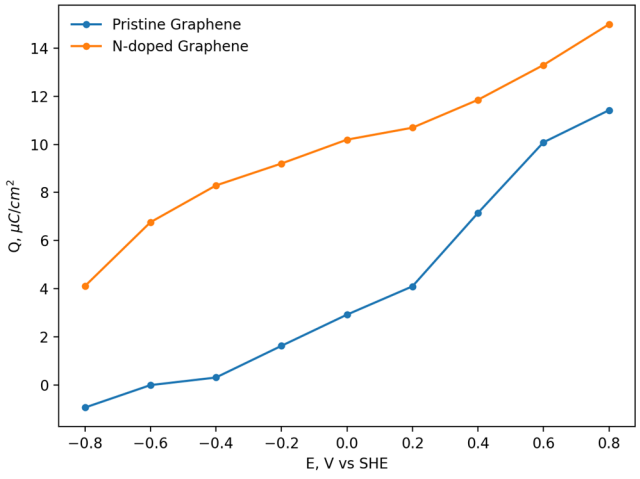

Figure 4. Dependence of surface charge density on potential for pristine and N-doped graphene, obtained using GC-DFT.

The potential of mean force exhibits several local minima. A minimum in the region of ~6 Å corresponds to a solvent-separated configuration of O_2 (Figure 3c). In this case, the molecule is not in direct contact with the surface but is instead separated from it by water molecules that are part of its solvation shell. The second minimum at a distance of ~3 Å corresponds to a physisorbed molecule (Figure 3d). Adsorption requires overcoming an energy barrier of 0.3 eV, which is associated with the partial desolvation of O_2 and the rearrangement of hydrogen bonds in water. The solvent contribution to the PMF (excluding the O_2–surface interaction) is shown in Figure S6 (Supplementary Materials) and is very similar to that of obtained for oxygen on a silver surface [34]. The physisorption state is 0.25 eV less energetically favorable compared to a fully solvated molecule. In the case of a hypothetical equilibrium between the bulk phase and the surface, this means that the concentration of physisorbed molecules is approximately 10^4 times lower than the concentration of solvent-separated molecules. Consequently, the surface is depleted of adsorbed molecular oxygen.

The local minimum closest to the surface, at a distance of ~2 Å, corresponds to chemisorbed species (Figure 3e). Chemisorbed oxygen possesses significantly higher energy than the physisorbed one, indicating that it is a metastable state, in accordance with Refs. [20,21]. A graphitic nitrogen reduces the chemisorption energy, which is in qualitative agreement with the work of Okamoto [20]. As shown in our previous work, a pyrrolic nitrogen exerts an even greater stabilizing effect, reducing the chemisorption energy to ~1 eV [22]. Okamoto also showed that as the number of nitrogen atoms, situated adjacent to the carbon atoms to which oxygen binds, increases, the chemisorption energy decreases, becoming even negative in configurations involving three or four nitrogen atoms [20]. However, the question remains as to whether such configurations can occur in real carbon materials, where the nitrogen concentration typically does not exceed a few percent [7,43–45]. In the Yu et al. work, which examines graphene with a relatively high concentration of graphitic nitrogen (~10%), the chemisorption energy is close to zero [11]. In our previous work, we showed that on N-doped graphenes with a low nitrogen concentration (~2%), the oxygen chemisorption energy decreases significantly as the potential decreases. However, a zero value is reached only at highly negative potentials, on the order of −0.8 V vs. SHE [22].

Summarizing our own findings and data from the literature, it can be concluded that an inner-sphere mechanism of the ORR (1–5) is possible either at high concentrations of nitrogen atoms, which are difficult to achieve experimentally, or at highly negative potentials. At low concentrations (on the order of a few percent) chemisorption does not occur. Even physisorbed oxygen has an energy 0.25 eV higher than that of a solvated molecule. Thus, the mechanism (6–10), which begins with outer-sphere electron transfer to a solvated oxygen molecule, is relevant and warrants analysis.

3.2. Free Energy Profile of the ORR on N-Doped Graphene

A comparison of the ORR free-energy profiles for the inner-sphere and outer-sphere mechanisms on the pristine and N-doped graphenes is shown in Figures 5a and 5b, respectively. The free energy of the first step of the outer-sphere mechanism (6) is given by:

$$\Delta G_6 = G_{O_2^-} - G_{O_2} - \mu_e$$

where $G_{O_2^-}$ and G_{O_2} are the free energies of the solvent-separated configuration of O_2 near the surface, and μ_e is the electrochemical potential of the electrons at the surface, which, in the CANDLE model, is given by the expression $\mu_e = -4.66\ \text{eV} - eU$ [41], where

U is the electrode potential vs. SHE. As shown in Figure 3 and other MD simulations [34,46,47], the free energy of a solvent-separated configuration of a solute is, to a good approximation, equal to its free energy in the bulk electrolyte and weakly depends on the type of surface or its charge. Therefore, for $G_{O_2^-}$ and G_{O_2}, we used the free energies of the molecules in the bulk electrolyte, calculated using the CANDLE model.

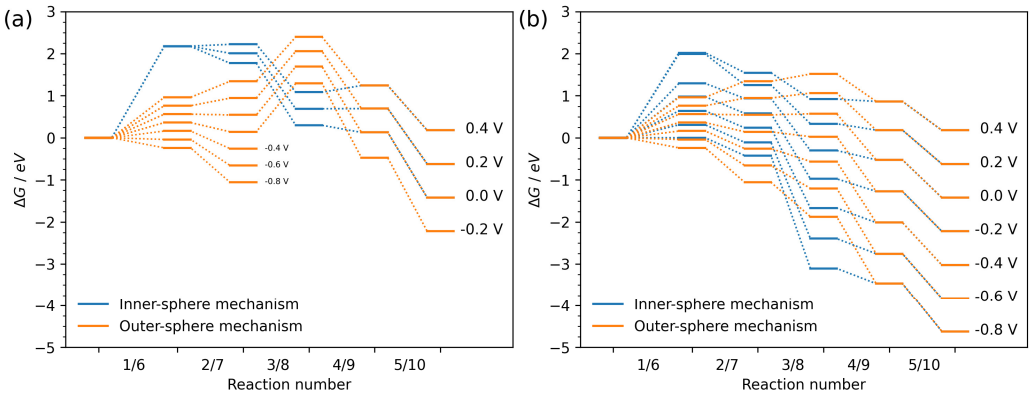

Figure 5. Free energy profiles for pristine (**a**) and N-doped (**b**) graphenes at different potentials. Blue and yellow profiles are for inner- and outer-sphere mechanisms respectively.

As shown by Ignaczak et al., the second reaction step (7) of the outer-sphere mechanism proceeds very rapidly due to a low reaction barrier of 0.06 eV [34]. In light of this, we assumed that the OOH^- ion at the first moment after the reaction step (7) is also solvated, like the O_2^- reactant. Therefore, we considered the solvated OOH^- ion within the electrolyte bulk when calculating the energy of reaction (7).

As shown in Figure 5b, the outer-sphere mechanism is energetically more favorable on the surface of N-doped graphene across the entire range of potentials considered, from 0.4 to −0.8 V. For pristine graphene, the complete energy profiles are presented for a narrower range of potentials (Figure 5a). In the case of the inner-sphere mechanism, this is because the chemisorbed *OOH intermediate becomes unstable at potentials below 0 V and spontaneously desorbs as an OOH^- ion, indicating that the ORR proceeds via a $2e^-$ mechanism. For the outer-sphere mechanism in Figure 5a, the complete ORR profile is shown only for potentials ranging from 0.4 to −0.2 V, because at more negative potentials, the configuration with two chemisorbed OH* intermediates also becomes unstable, rendering the $4e^-$ mechanism impossible. At potentials greater than −0.2 V, the third reaction of the outer-sphere mechanism (7) on defect-free graphene is highly endothermic; this is due to the significantly higher chemisorption energy of OH* compared to that on N-doped graphene. Thus, we suppose that on defect-free graphene the outer-sphere mechanism terminates at reaction (7) regardless of the potential, and the number of electrons transferred per oxygen molecule is 2. It also follows from Figure 5 that, for an outer-sphere mechanism, the catalytic effect of nitrogen impurities consists of stabilizing a configuration with two chemisorbed OH* species. This renders step (7) isoergonic at a potential of approximately 0 V and initiates the ORR via a $4e^-$ mechanism.

From Figure 5b, we have determined that the free energy of the first reaction in the outer-sphere mechanism is given by $\Delta G_6 = 0.56\ \text{eV} + eU$. It follows that the calculated standard redox potential for the O_2/O_2^- process (at which $\Delta G_6 = 0$) is −0.56 V vs. SHE, whereas the experimental value is more positive, −0.33 V [48]. This discrepancy may be explained by an error of ~0.1 eV, with which the CANDLE model reproduces solvation energies of solutes, as well as by an error of ~0.1 eV in determining the SHE level ($\mu_e^{SHE} = -4.66$ eV) [36]. The fact that the experimental value of the standard redox potential of O_2/O_2^- is more positive indicates that the outer-sphere mechanism is even more

energetically favorable than predicted by GC-DFT calculations, and the free energy profile becomes "downhill" not at a potential of −0.56 V, but rather at a potential on the order of −0.3 V. However, this value differs from the experimental onset potential for nitrogen-doped carbon materials in an alkaline medium, which is typically more positive—on the order of 0 V vs. SHE [7,25,42]. This can be explained by the kinetics of reaction (7), as proposed by Schmickler's group [34]. If step (7) proceeds rapidly (as discussed above) the concentration of superoxide ions O_2^- must be low, and the formal potential of the reaction (6) shifts toward a more positive range. For instance, if the O_2^- concentration is 10^{-6} M, the formal potential is on the order of zero.

Before concluding, we should note some limitations of our calculations. In this work, we considered only graphitic N, as it is the most extensively studied type of nitrogen in computational research. However, other configurations, such as pyridinic and pyrrolic nitrogen, can also serve as active sites [3]. In the outer-sphere mechanism considered in this work, the thermodynamics of the 2e pathway (as opposed to the 4e pathway) is independent of the catalytic surface, since the first two reactions, (6) and (7), do not involve the chemisorption of intermediates. Thus, the data in Figure 5 for reactions (6) and (7) are applicable to various defects. Comparing these data with the thermodynamics of the inner-sphere reaction mechanism, calculated in our previous work [22], one can conclude that, at least for the 2e pathway, the outer-sphere mechanism is also more favorable for both pyridine and pyrrole nitrogen atoms. This makes further research relevant for generalizing the findings of our work to various types of nitrogen.

It should also be noted that the thermodynamic calculations performed in this work constitute an important and highly common stage in the analysis of catalytic reactions. However, a complete analysis requires kinetic data for each elementary step [49]. From our perspective, it is most important to compare the kinetics of the most energetically demanding reactions. For N-doped graphene and both mechanisms considered, this is the first reaction, as it becomes exothermic at more negative potentials than the other reactions. The barrier for the reaction (1) is 1.23 eV, 0.99 eV, and 0.76 eV at potentials of 0, −0.2, and −0.4 V vs. SHE, respectively [28]. The barrier for the outer-sphere electron transfer (6) at the equilibrium potential is lower, ~0.5 eV [33]. Consequently, we believe the outer-sphere mechanism is more favorable not only from a thermodynamic perspective but also from a kinetic one. Let us also note that nitrogen dopants accelerate outer-sphere electron transfer by altering the electronic properties of graphene and enhancing the coupling between O_2 and the catalyst [50]. This should be considered an additional factor explaining the catalytic activity of nitrogen impurities when the reaction proceeds via an outer-sphere mechanism.

Finally, our calculations implicitly assumed that the catalytic surface was clean. In reality, the active sites may be predominantly occupied by one of the intermediates that is bound too strongly to the surface. Verifying this requires additional microkinetic modeling.

4. Conclusions

Combined MD and DFT calculations have shown that both the physisorption and chemisorption of an oxygen molecule near a graphitic N atom in graphene are endothermic reactions, which promotes the ORR proceeding via an outer-sphere mechanism. Based on GC-DFT calculations, it was shown that in an alkaline environment, the outer-sphere mechanism proposed by the Schmickler's group for gold is energetically more favorable than the inner-sphere associative mechanism for N-doped graphene with graphitic nitrogen atoms. The catalytic effect of nitrogen impurities lies in lowering the chemisorption energy of the *OH intermediate, which initiates the reaction via a four-electron mechanism, in contrast to pristine graphene, where the reaction terminates after the

transfer of two electrons. Based on an analysis of literature data, it is supposed that at high concentrations of nitrogen impurities and highly negative potentials—conditions under which the oxygen adsorption/chemisorption becomes exothermic—the ORR proceeds via the generally accepted inner-sphere mechanism.

Supplementary Materials: The following supporting information can be downloaded at https://www.mdpi.com/article/10.3390/nano16231521/s1: Figure S1. Five specific directions along which the energy of the H_2O–O_2 pair was scanned. Figure S2. DFT energy profiles along five specific directions (shown in Figure S1) and their MD approximations. Table S1. Buckingham potential parameters describing the interaction between water atoms and atoms of an oxygen molecule. Figure S3. Atomic charges in N-doped graphene for the uncharged surface (left) and for the charged surface at a potential of 0 V vs. SHE (right), obtained using the DDEC6 method. Figure S4. Optimized positions of a water molecule for four random initial placements on the surface of pristine (left) and N-doped graphene (right). Figure S5. Interaction energy between graphene and a water molecule for pristine (left) and Ndoped (right) graphene, calculated using DFT and MD methods. Here, the position of the DFT energy minimum is taken as zero on the x-axis. Table S2. Buckingham potential for water-graphene interaction. Figure S6. The solvent contribution to the PMF (excluding the O_2—surface interaction) at PZC and $E = 0$. Figure S7. The convergence tests for the plane-wave cutoff (left) and k-point sampling (right).

Author Contributions: S.K.: supervision, conceptualization, and writing—original draft preparation. V.K.: DFT calculations. P.C.: force-field development. S.P.: MD simulations. All authors have read and agreed to the published version of the manuscript.

Funding: This work was supported by the Ministry of Science and Higher Education of the Russian Federation (State Assignment No. 075-00270-26-00).

Data Availability Statement: Data is contained within the article or supplementary material: The original contributions presented in this study are included in the article/supplementary material. Further inquiries can be directed to the corresponding author(s).

Conflicts of Interest: The authors declare no conflicts of interest.

Abbreviations

The following abbreviations are used in this manuscript:

GC-DFT	Grand-canonical density function theory
MD	Molecular dynamics
ORR	Oxygen reduction reaction
SHE	Standard hydrogen electrode
CMFECs	Metal-free carbon-based electrocatalysts
PZC	Potential of zero charge

References

1. Gong, K.; Du, F.; Xia, Z.; Durstock, M.; Dai, L. Nitrogen-Doped Carbon Nanotube Arrays with High Electrocatalytic Activity for Oxygen Reduction. *Science* **2009**, *323*, 760–764. https://doi.org/10.1126/science.1168049.
2. Gao, R.; Zhang, S.; Huang, X.; Zhang, J.; Yang, Q.; Xiao, Z.; Zhao, S. Rational Design of Carbon-Based Metal-Free Electrocatalyst Architectures for Selective Oxygen Reduction Reaction: From Structure–Performance Correlations to Predictive Strategies. *Nano Res.* **2026**, *19*, 94908907. https://doi.org/10.26599/NR.2026.94908907.
3. Islam, M.S.; Islam, M.R.; Ahmed, M.S.; Mahmud, M.A. A Review on Carbon-Based Metal-Free Electrocatalysts for Energy-Related ORR in Alkaline Medium. *Adv. Mater. Sci. Eng.* **2025**, *2025*, 4114894. https://doi.org/10.1155/amse/4114894.
4. Rauf, M.; Zhao, Y.-D.; Wang, Y.-C.; Zheng, Y.-P.; Chen, C.; Yang, X.-D.; Zhou, Z.-Y.; Sun, S.-G. Insight into the Different ORR Catalytic Activity of Fe/N/C between Acidic and Alkaline Media: Protonation of Pyridinic Nitrogen. *Electrochem. Commun.* **2016**, *73*, 71–74. https://doi.org/10.1016/j.elecom.2016.10.016.

5. Herranz, J.; Jaouen, F.; Lefèvre, M.; Kramm, U.I.; Proietti, E.; Dodelet, J.-P.; Bogdanoff, P.; Fiechter, S.; Abs-Wurmbach, I.; Bertrand, P.; et al. Unveiling N-Protonation and Anion-Binding Effects on Fe/N/C Catalysts for O 2 Reduction in Proton-Exchange-Membrane Fuel Cells. *J. Phys. Chem. C* **2011**, *115*, 16087–16097. https://doi.org/10.1021/jp2042526.
6. Wan, K.; Yu, Z.; Li, X.; Liu, M.; Yang, G.; Piao, J.; Liang, Z. pH Effect on Electrochemistry of Nitrogen-Doped Carbon Catalyst for Oxygen Reduction Reaction. *ACS Catal.* **2015**, *5*, 4325–4332. https://doi.org/10.1021/acscatal.5b01089.
7. Begum, H.; Ahmed, M.S.; Kim, Y.-B. Nitrogen-Rich Graphitic-Carbon@graphene as a Metal-Free Electrocatalyst for Oxygen Reduction Reaction. *Sci. Rep.* **2020**, *10*, 12431. https://doi.org/10.1038/s41598-020-68260-3.
8. Lv, Q.; Si, W.; He, J.; Sun, L.; Zhang, C.; Wang, N.; Yang, Z.; Li, X.; Wang, X.; Deng, W.; et al. Selectively Nitrogen-Doped Carbon Materials as Superior Metal-Free Catalysts for Oxygen Reduction. *Nat. Commun.* **2018**, *9*, 3376. https://doi.org/10.1038/s41467-018-05878-y.
9. Pham, N.N.T.; Kim, K.H.; Han, B.; Lee, S.G. Theoretical Investigation of the Active Sites in N-Doped Graphene Bilayer for the Oxygen Reduction Reaction in Alkaline Media in PEMFCs. *J. Phys. Chem. C* **2022**, *126*, 5863–5872. https://doi.org/10.1021/acs.jpcc.1c09657.
10. Ricca, C.; Labat, F.; Zavala, C.; Russo, N.; Adamo, C.; Merino, G.; Sicilia, E. B,N-Codoped Graphene as Catalyst for the Oxygen Reduction Reaction: Insights from Periodic and Cluster DFT Calculations. *J. Comput. Chem.* **2018**, *39*, 637–647. https://doi.org/10.1002/jcc.25148.
11. Yu, L.; Pan, X.; Cao, X.; Hu, P.; Bao, X. Oxygen Reduction Reaction Mechanism on Nitrogen-Doped Graphene: A Density Functional Theory Study. *J. Catal.* **2011**, *282*, 183–190. https://doi.org/10.1016/j.jcat.2011.06.015.
12. Yan, X.; Liu, H.; Jia, Y.; Zhang, L.; Xu, W.; Wang, X.; Chen, J.; Yang, D.; Yao, X. Clarifying the Origin of Oxygen Reduction Activity in Heteroatom-Modified Defective Carbon. *Cell Rep. Phys. Sci.* **2020**, *1*, 100083. https://doi.org/10.1016/j.xcrp.2020.100083.
13. Tai, S.-H.; Chang, B.K. Effect of Nitrogen-Doping Configuration in Graphene on the Oxygen Reduction Reaction. *RSC Adv.* **2019**, *9*, 6035–6041. https://doi.org/10.1039/C8RA08576E.
14. Zhang, L.; Xia, Z. Mechanisms of Oxygen Reduction Reaction on Nitrogen-Doped Graphene for Fuel Cells. *J. Phys. Chem. C* **2011**, *115*, 11170–11176. https://doi.org/10.1021/jp201991j.
15. Yan, H.J.; Xu, B.; Shi, S.Q.; Ouyang, C.Y. First-Principles Study of the Oxygen Adsorption and Dissociation on Graphene and Nitrogen Doped Graphene for Li-Air Batteries. *J. Appl. Phys.* **2012**, *112*, 104316. https://doi.org/10.1063/1.4766919.
16. Ni, S.; Li, Z.; Yang, J. Oxygen Molecule Dissociation on Carbon Nanostructures with Different Types of Nitrogen Doping. *Nanoscale* **2012**, *4*, 1184–1189. https://doi.org/10.1039/C1NR11086A.
17. Nørskov, J.K.; Rossmeisl, J.; Logadottir, A.; Lindqvist, L.; Kitchin, J.R.; Bligaard, T.; Jónsson, H. Origin of the Overpotential for Oxygen Reduction at a Fuel-Cell Cathode. *J. Phys. Chem. B* **2004**, *108*, 17886–17892. https://doi.org/10.1021/jp047349j.
18. Gao, G.; Wang, L.-W. Substantial Potential Effects on Single-Atom Catalysts for the Oxygen Evolution Reaction Simulated via a Fixed-Potential Method. *J. Catal.* **2020**, *391*, 530–538. https://doi.org/10.1016/j.jcat.2020.08.032.
19. Kim, D.; Shi, J.; Liu, Y. Substantial Impact of Charge on Electrochemical Reactions of Two-Dimensional Materials. *J. Am. Chem. Soc.* **2018**, *140*, 9127–9131. https://doi.org/10.1021/jacs.8b03002.
20. Okamoto, Y. First-Principles Molecular Dynamics Simulation of O2 Reduction on Nitrogen-Doped Carbon. *Appl. Surf. Sci.* **2009**, *256*, 335–341. https://doi.org/10.1016/j.apsusc.2009.08.027.
21. Sorescu, D.C.; Jordan, K.D.; Avouris, P. Theoretical Study of Oxygen Adsorption on Graphite and the (8,0) Single-Walled Carbon Nanotube. *J. Phys. Chem. B* **2001**, *105*, 11227–11232. https://doi.org/10.1021/jp0122979.
22. Kislenko, V.A.; Pavlov, S.V.; Nikitina, V.A.; Kislenko, S.A. Revision of the Oxygen Reduction Reaction on N-Doped Graphenes by Grand-Canonical DFT. *Phys. Chem. Chem. Phys.* **2024**, *26*, 293–303. https://doi.org/10.1039/D3CP04517J.
23. Kislenko, V.A.; Pavlov, S.V.; Kislenko, S.A. Thermodynamics of the Oxygen Reduction Reaction on Surfaces of Nitrogen-Doped Graphene. *Russ. J. Phys. Chem. A* **2023**, *97*, 2354–2361. https://doi.org/10.1134/S0036024423110158.
24. Li, M.F.; Liao, L.W.; Yuan, D.F.; Mei, D.; Chen, Y.-X. pH Effect on Oxygen Reduction Reaction at Pt(111) Electrode. *Electrochim. Acta* **2013**, *110*, 780–789. https://doi.org/10.1016/j.electacta.2013.04.096.
25. Behan, J.A.; Iannaci, A.; Domínguez, C.; Stamatin, S.N.; Hoque, M.K.; Vasconcelos, J.M.; Perova, T.S.; Colavita, P.E. Electrocatalysis of N-Doped Carbons in the Oxygen Reduction Reaction as a Function of pH: N-Sites and Scaffold Effects. *Carbon N. Y.* **2019**, *148*, 224–230. https://doi.org/10.1016/j.carbon.2019.03.052.
26. CHEN, Y.; CHEN, Q.; ZHENG, Y.; KANG, J.; LIAO, L. pH Effect on Oxygen Reduction Reaction at Polycrystalline Au Electrode. *Sci. Sin. Chim.* **2011**, *41*, 1777–1783. https://doi.org/10.1360/032011-426.

27. Koper, M.T.M. Theory of Multiple Proton–Electron Transfer Reactions and Its Implications for Electrocatalysis. *Chem. Sci.* **2013**, *4*, 2710. https://doi.org/10.1039/c3sc50205h.
28. Kislenko, V.A.; Pavlov, S.V.; Kislenko, S.A. Potential-Dependent Kinetics of Oxygen Chemisorption as the Crucial Step of Oxygen Reduction Reaction: GCDFT Study. *J. Electroanal. Chem.* **2024**, *974*, 118708. https://doi.org/10.1016/j.jelechem.2024.118708.
29. Ignaczak, A.; Santos, E.; Schmickler, W. Oxygen Reduction Reaction on Gold in Alkaline Solutions—The Inner or Outer Sphere Mechanisms in the Light of Recent Achievements. *Curr. Opin. Electrochem.* **2019**, *14*, 180–185. https://doi.org/10.1016/j.coelec.2018.07.011.
30. Yang, H.-H.; McCreery, R.L. Elucidation of the Mechanism of Dioxygen Reduction on Metal-Free Carbon Electrodes. *J. Electrochem. Soc.* **2000**, *147*, 3420. https://doi.org/10.1149/1.1393915.
31. Quaino, P.; Luque, N.B.; Nazmutdinov, R.; Santos, E.; Schmickler, W. Why Is Gold Such a Good Catalyst for Oxygen Reduction in Alkaline Media? *Angew. Chem. Int. Ed.* **2012**, *51*, 12997–13000. https://doi.org/10.1002/anie.201205902.
32. Goduljan, A.; de Campos Pinto, L.M.; Juarez, F.; Santos, E.; Schmickler, W. Oxygen Reduction on Ag(100) in Alkaline Solutions—A Theoretical Study. *ChemPhysChem* **2016**, *17*, 500–505. https://doi.org/10.1002/cphc.201501036.
33. Ignaczak, A.; Nazmutdinov, R.; Goduljan, A.; de Campos Pinto, L.M.; Juarez, F.; Quaino, P.; Santos, E.; Schmickler, W. A Scenario for Oxygen Reduction in Alkaline Media. *Nano Energy* **2016**, *29*, 362–368. https://doi.org/10.1016/j.nanoen.2016.11.009.
34. Ignaczak, A.; Nazmutdinov, R.; Goduljan, A.; de Campos Pinto, L.M.; Juarez, F.; Quaino, P.; Belletti, G.; Santos, E.; Schmickler, W. Oxygen Reduction in Alkaline Media—A Discussion. *Electrocatalysis* **2017**, *8*, 554–564. https://doi.org/10.1007/s12678-017-0365-y.
35. Sundararaman, R.; Letchworth-Weaver, K.; Schwarz, K.A.; Gunceler, D.; Ozhabes, Y.; Arias, T.A. JDFTx: Software for Joint Density-Functional Theory. *SoftwareX* **2017**, *6*, 278–284. https://doi.org/10.1016/j.softx.2017.10.006.
36. Sundararaman, R.; Goddard, W.A. The Charge-Asymmetric Nonlocally Determined Local-Electric (CANDLE) Solvation Model. *J. Chem. Phys.* **2015**, *142*, 64107. https://doi.org/10.1063/1.4907731.
37. Perdew, J.P.; Burke, K.; Ernzerhof, M. Generalized Gradient Approximation Made Simple. *Phys. Rev. Lett.* **1996**, *77*, 3865–3868. https://doi.org/10.1103/PhysRevLett.77.3865.
38. Grimme, S.; Antony, J.; Ehrlich, S.; Krieg, H. A Consistent and Accurate Ab Initio Parametrization of Density Functional Dispersion Correction (DFT-D) for the 94 Elements H-Pu. *J. Chem. Phys.* **2010**, *132*, 154104. https://doi.org/10.1063/1.3382344.
39. Garrity, K.F.; Bennett, J.W.; Rabe, K.M.; Vanderbilt, D. Pseudopotentials for High-Throughput DFT Calculations. *Comput. Mater. Sci.* **2014**, *81*, 446–452. https://doi.org/10.1016/j.commatsci.2013.08.053.
40. Bhattacharjee, J. Activation of Graphenic Carbon Due to Substitutional Doping by Nitrogen: Mechanistic Understanding from First Principles. *J. Phys. Chem. Lett.* **2015**, *6*, 1653–1660. https://doi.org/10.1021/acs.jpclett.5b00304.
41. Gunceler, D.; Letchworth-Weaver, K.; Sundararaman, R.; Schwarz, K.A.; Arias, T.A. The Importance of Nonlinear Fluid Response in Joint Density-Functional Theory Studies of Battery Systems. *Model. Simul. Mat. Sci. Eng.* **2013**, *21*, 74005. https://doi.org/10.1088/0965-0393/21/7/074005.
42. Yang, H. Bin; Miao, J.; Hung, S.-F.; Chen, J.; Tao, H.B.; Wang, X.; Zhang, L.; Chen, R.; Gao, J.; Chen, H.M.; et al. Identification of Catalytic Sites for Oxygen Reduction and Oxygen Evolution in N-Doped Graphene Materials: Development of Highly Efficient Metal-Free Bifunctional Electrocatalyst. *Sci. Adv.* **2016**, *2*, e1501122. https://doi.org/10.1126/sciadv.1501122.
43. Zheng, Y.; Jiao, Y.; Ge, L.; Jaroniec, M.; Qiao, S.Z. Two-Step Boron and Nitrogen Doping in Graphene for Enhanced Synergistic Catalysis. *Angew. Chem.* **2013**, *125*, 3192–3198. https://doi.org/10.1002/ange.201209548.
44. Liang, J.; Jiao, Y.; Jaroniec, M.; Qiao, S.Z. Sulfur and Nitrogen Dual-Doped Mesoporous Graphene Electrocatalyst for Oxygen Reduction with Synergistically Enhanced Performance. *Angew. Chem. Int. Ed.* **2012**, *51*, 11496–11500. https://doi.org/10.1002/anie.201206720.
45. Lai, L.; Potts, J.R.; Zhan, D.; Wang, L.; Poh, C.K.; Tang, C.; Gong, H.; Shen, Z.; Lin, J.; Ruoff, R.S. Exploration of the Active Center Structure of Nitrogen-Doped Graphene-Based Catalysts for Oxygen Reduction Reaction. *Energy Environ. Sci.* **2012**, *5*, 7936–7942. https://doi.org/10.1039/C2EE21802J.
46. Sun, Q. The Interplay between Hydrophobic and Solute–Solute Interactions: Implications for Hofmeister Effects. *Chem. Phys. Impact* **2026**, *12*, 101073. https://doi.org/10.1016/j.chphi.2026.101073.
47. Ivaništšev, V.; Méndez-Morales, T.; Lynden-Bell, R.M.; Cabeza, O.; Gallego, L.J.; Varela, L.M.; Fedorov, M.V. Molecular Origin of High Free Energy Barriers for Alkali Metal Ion Transfer through Ionic Liquid–Graphene Electrode Interfaces. *Phys. Chem. Chem. Phys.* **2016**, *18*, 1302–1310. https://doi.org/10.1039/C5CP05973A.
48. Ilan, Y.A.; Czapski, G.; Meisel, D. The One-Electron Transfer Redox Potentials of Free Radicals. I. The Oxygen/Superoxide System. *Biochim. ET Biophys. Acta (BBA) Bioenerg.* **1976**, *430*, 209–224. https://doi.org/10.1016/0005-2728(76)90080-3.
49. Oberhofer, H. Electrocatalysis Beyond the Computational Hydrogen Electrode. In *Handbook of Materials Modeling*; Springer International Publishing: Cham, Switzerland, 2020; pp. 1505–1537.

50. Doronin, S.V.; Budkov, Y.A.; Itkis, D.M. Electrocatalytic Activity of Doped Graphene: Quantum-Mechanical Theory View. *Carbon N. Y.* **2021**, *175*, 202–214. https://doi.org/10.1016/j.carbon.2021.01.020.

Disclaimer/Publisher's Note: The statements, opinions and data contained in all publications are solely those of the individual author(s) and contributor(s) and not of MDPI and/or the editor(s). MDPI and/or the editor(s) disclaim responsibility for any injury to people or property resulting from any ideas, methods, instructions or products referred to in the content.